CHEMISTRY
A EUROPEAN JOURNAL

DOI: 10.1002/chem.200600934

Functionalization of Heteropolyanions—Osmium and Rhenium Nitrido Derivatives of Keggin- and Dawson-Type Polyoxotungstates: Synthesis, Characterization and Multinuclear (^{183}W, ^{15}N) NMR, EPR, IR, and UV/Vis Fingerprints

Céline Dablemont,[a] Christopher G. Hamaker,[b, c] René Thouvenot,[a] Zbigniew Sojka,[d] Michel Che,[e] Eric A. Maatta,*[b] and Anna Proust*[a]

Abstract: Reaction of $K_{10}[\alpha_2\text{-}P_2W_{17}O_{61}]$ or $K_{10}[\alpha_1\text{-}P_2W_{17}O_{61}]$ or $[Bu_4N][OsCl_4N]$ in a water/methanol mixture, and subsequent precipitation with $(Bu_4N)Br$ provided $[\alpha_2\text{-}P_2W_{17}O_{61}\{Os^{VI}N\}]^{7-}$ and $[\alpha_1\text{-}P_2W_{17}O_{61}\{Os^{VI}N\}]^{7-}$ Dawson structures as tetrabutylammonium salts. Reactions of $[(Bu_4N)_4][\alpha\text{-}H_3PW_{11}O_{39}]$ with either $[ReCl_3(N_2Ph_2)(PPh_3)_2]$ or $[Bu_4N][ReCl_4N]$ are alternatives to the synthesis of $[(Bu_4N)_4][\alpha\text{-}PW_{11}O_{39}\{Re^{VI}N\}]$. ^{183}W and ^{15}N NMR, EPR, IR, and UV-visible spectroscopies and cyclic voltammetry have been used to characterize these compounds and the corresponding $[(Bu_4N)_4][\alpha\text{-}PW_{11}O_{39}\{Os^{VI}N\}]$ Keggin derivative.

Keywords: EPR spectroscopy · nitrido · NMR spectroscopy · osmium · polyoxometalates · rhenium · tungsten

Introduction

Early transition-metal–oxygen-anion clusters (polyoxometalates or POMs) are remarkable because of their molecular and electronic tunability, and their range of properties and applications, which are unmatched by any other class of compounds. In particular, POM-based molecular materials are a rapidly growing class of compounds.[1–5] Most of them are class I hybrid materials, that is, they are based on weak, noncovalent interactions between the POM and the organic component(s).[6] Hybrid salts based upon organic π-electron donors and POMs[7] and macrocation–POM ionic crystals[8,9] are two representative examples. Class II materials, in which the POM component is covalently grafted into an organic matrix, are comparatively less developed, although the field is being explored by some of us and others.[10–13] Because the synthesis of class II POM-based materials requires prior covalent derivatization of the POM, it can be expected that their development will parallel progress in the functionalization of POMs. Building on our experience in the functionalization of Lindqvist-type POMs,[11,14–20] we turned towards the functionalization of the more attractive Keggin- and Dawson-type POMs. However, the synthetic methodology that proved successful in the Lindqvist series is not easily extended to the Keggin and Dawson species. Thus, a metathetical approach using organic isocyanates RN=C=O

[a] Dr. C. Dablemont, Dr. R. Thouvenot, Prof. Dr. A. Proust
Université Pierre et Marie Curie-Paris6
Institut de Chimie Moléculaire FR 2769
Laboratoire de Chimie Inorganique et Matériaux Moléculaires UMR CNRS 7071
4 Place Jussieu, Case 42, 75252 Paris Cedex 05 (France)
Fax: (+33) 144-273-841
E-mail: proust@ccr.jussieu.fr

[b] Dr. C. G. Hamaker, Prof. Dr. E. A. Maatta
Department of Chemistry, Kansas State University
Manhattan, Kansas 66506-3701 (USA)
Fax: (+1) 785-532-6666
E-mail: eam@ksu.edu

[c] Dr. C. G. Hamaker
Present address: Department of Chemistry
Illinois State University, Normal, IL 61790-4160 (USA)

[d] Prof. Dr. Z. Sojka
Regional Laboratory of Physicochemical Analyses and Structural Research, ul. Ingardena 3, 30-060 Krakow (Poland)
and
Faculty of Chemistry, Jagiellonian University
ul. Ingardena 3, 30-060 Krakow (Poland)

[e] Prof. Dr. M. Che
Université Pierre et Marie Curie-Paris 6
Institut Universitaire de France
Laboratoire de Réactivité de Surface UMR CNRS 7609
4 Place Jussieu, Case 178, 75252 Paris Cedex 05 (France)

(based on the analogy between the Mo=O and the C=O functions), which provides a convenient means of functionalization of $[Mo_6O_{19}]^{2-}$, is hampered by competitive reduction processes in the case of $[PM_{11}O_{39}\{MoO\}]^{3-}$ (M = Mo, W).[15,21] To date, the reaction between a preformed lacunary polyanion and a coordination complex bearing the desired function appears to be the most convenient route to functionalized Keggin- and Dawson-type POMs. Thus the reaction of $[H_3PW_{11}O_{39}]^{4-}$ with $[ReCl_3(NPh)(PPh_3)_3]$ in acetonitrile in the presence of NEt_3 has provided the first Keggin-type organoimido derivative $[PW_{11}O_{39}\{ReNC_6H_5\}]^{4-}$.[22]

We then turned our attention towards the synthesis of nitrido derivatives for the following reasons: 1) they could serve as precursors to other nitrogenous derivatives through reactions with electrophiles or nucleophiles: organoimido derivatives would thus result from the reaction of alkylating reagents on the nitrido function;[23] 2) a renewal of interest in nitrido compounds in the context of nitrogen fixation as recently described by Schrock and Yandulov;[24,25] 3) nitrido derivatives have demonstrated utility in N-atom transfer reactions to organic substrates. In view of the activity of porphyrin,[26,27] corrole,[28–30] and Schiff base complexes[31,32] in aziridination of alkenes and amidation of saturated C–H bonds, and on considering the intriguing analogy of transition-metal-substituted POMs to metalloporphyrins, nitrido-functionalized POMs are of special interest. Yet only two nitrido derivatives of POMs[33,34] were mentioned prior to our preliminary report on $[PW_{11}O_{39}\{Re^{VI}N\}]^{4-}$ and $[PW_{11}O_{39}\{Os^{VI}N\}]^{4-}$.[35] In this contribution we will discuss various routes to $[PW_{11}O_{39}\{Re^{VI}N\}]^{4-}$, describe the syntheses of the α_1 and α_2 isomers of $[P_2W_{17}O_{61}\{Os^{VI}N\}]^{7-}$, report ^{183}W and ^{15}N NMR spectroscopic characterization of $[PW_{11}O_{39}\{Os^{VI}N\}]^{4-}$, $[\alpha_2\text{-}P_2W_{17}O_{61}\{Os^{VI}N\}]^{7-}$, and $[\alpha_1\text{-}P_2W_{17}O_{61}\{Os^{VI}N\}]^{7-}$, and outline a complete analysis of the EPR spectrum of $[PW_{11}O_{39}\{Re^{VI}N\}]^{4-}$. In addition, as the relationship between structure and ^{183}W chemical shift in POMs remains to be established, the ^{183}W NMR spectra of $[PW_{11}O_{39}\{Os^{VI}N\}]^{4-}$ and $[\alpha_2\text{-}P_2W_{17}O_{61}\{Os^{VI}N\}]^{7-}$ have been assigned precisely in order to collect as much ^{183}W data as possible.

Results and Discussion

Synthesis: A great number of d^n transition-metal-substituted POMs can be obtained from monovacant POMs, especially the Keggin- and Dawson-type tungstophosphates. The method can be used for the preparation of oxo, for example, $[\alpha\text{-}PW_{11}O_{39}\{Re^{V}O\}]^{4-}$[36] and $[\alpha\text{-}PW_{11}O_{39}\{Mo^{V}O\}]^{4-}$,[37,38] and organoimido $[\alpha\text{-}PW_{11}O_{39}\{Re^{V}(NPh)\}]^{4-}$[22] derivatives. The method also applies to the synthesis of the nitrido-functionalized POMs: it was first used to prepare $[\alpha\text{-}PW_{11}O_{39}\{TcN\}]^{4-}$[34] and has now been extended to the synthesis of $[\alpha\text{-}PW_{11}O_{39}\{Re^{VI}N\}]^{4-}$, $[\alpha\text{-}PW_{11}O_{39}\{Os^{VI}N\}]^{4-}$, $[\alpha_2\text{-}P_2W_{17}O_{61}\{Os^{VI}N\}]^{7-}$, and $[\alpha_1\text{-}P_2W_{17}O_{61}\{Os^{VI}N\}]^{7-}$. These last four compounds have been obtained by reaction of the monovacant species $[\alpha\text{-}PW_{11}O_{39}]^{7-}$, $[\alpha_2\text{-}P_2W_{17}O_{61}]^{10-}$, or $[\alpha_1\text{-}P_2W_{17}O_{61}]^{10-}$ with the nitrido complexes $[ReCl_4N]^-$ or $[OsCl_4N]^-$, either in aqueous solution or in acetonitrile, and have been isolated as $[Bu_4N]^+$ salts.

At the beginning of our work on nitrido-functionalized Keggin-type POMs, the reaction between $[(Bu_4N)_4][\alpha\text{-}H_3PW_{11}O_{39}]$ and $[ReCl_2N(PPh_3)_2]$ in CH_3CN appeared to be the most convenient way to prepare $[(Bu_4N)_4][\alpha\text{-}PW_{11}O_{39}\{Re^{VI}N\}]$.[35] However, adventitious contamination by $[(Bu_4N)_4][\alpha\text{-}PW_{11}O_{39}\{Re^{V}O\}]$, probably as a result of impurities in $[ReCl_2N(PPh_3)_2]$, was revealed by a sharp ^{31}P NMR spectroscopic signal at $\delta = -14.59$ ppm in CD_3CN/CH_3CN. Purification of the contaminated samples has been achieved by means of column chromatography on silica gel, by using a mixture of CH_2Cl_2/CH_3CN (1:1) as the eluent. Nevertheless, there are other routes to obtain $[(Bu_4N)_4][\alpha\text{-}PW_{11}O_{39}\{Re^{VI}N\}]$ and a more pure sample has been prepared by the reaction between $[(Bu_4N)_4][\alpha\text{-}H_3PW_{11}O_{39}]$ and $[Bu_4N][ReCl_4N]$[39] in CH_3CN, as described in the Experimental Section. Moreover, in our search for hydrazido-functionalized Keggin-type POMs, we found that the reaction between $[ReCl_3(N_2Ph_2)(PPh_3)_2]$[40] and $[\alpha\text{-}H_3PW_{11}O_{39}]^{4-}$ does not yield the targeted hydrazido derivative, but instead results in the formation of $[(Bu_4N)_4][\alpha\text{-}PW_{11}O_{39}\{Re^{VI}N\}]$ through cleavage of the nitrogen–nitrogen bond. It was identified from its electrospray ionization (ESI) mass spectrum (see below) and by a broad ^{31}P NMR spectroscopic signal at $\delta = -19$ ppm in CD_3CN/CH_3CN,[35] whereas $[(Bu_4N)_4][\alpha\text{-}PW_{11}O_{39}\{Re^{VI}O\}]$ is characterized by a broad signal at $\delta = -18$ ppm.[21] It is worth noting that the synthesis of $[ReCl_2N(PPh_3)_2]$, from $K[ReO_4]$ or $[ReCl_3O(PPh_3)_2]$ and either hydrazinium dichloride[41] or phenylhydrazinium chloride,[42] relies on such nitrogen–nitrogen bond breaking.

IR spectroscopy: The IR spectra of $[(Bu_4N)_4][\alpha\text{-}PW_{11}O_{39}\{Os^{VI}N\}]$ and $[(Bu_4N)_4][\alpha\text{-}PW_{11}O_{39}\{Re^{VI}N\}]$ are quite similar and display the characteristic features of a Keggin-type structure: four strong bands are indeed observed, at 1072, 963 (961), 884 (881), and 811 (802) cm^{-1}, which are assigned to the $\tilde{\nu}$(PO), $\tilde{\nu}$(M=O), and $\tilde{\nu}$(M–O–M) stretching modes, respectively.[43–45]

The IR spectrum of $[(Bu_4N)_7][\alpha_2\text{-}P_2W_{17}O_{61}\{Os^{VI}N\}]$ displays the characteristic features of a Dawson-type structure: four strong bands at 1089, 955, 911, and 786 cm^{-1}, which correspond to the $\tilde{\nu}$(PO), $\tilde{\nu}$(M=O), and $\tilde{\nu}$(M–O–M) stretching modes, respectively.[46,47]

In all cases, the observation of only one strong band between 1100 and 1050 cm^{-1}, assigned to the antisymmetric stretching of the PO_4 tetrahedron, implies a relatively strong interaction between the addendum metal and the oxygen atom of the phosphate group.[48]

UV-visible spectroscopy: The electronic spectrum of $[(Bu_4N)_7][\alpha_2\text{-}P_2W_{17}O_{61}\{Os^{VI}N\}]$ in acetonitrile displays a very broad band at $\lambda = 455$ nm assigned to the d–d transition that is also observed at 466 nm for $[Bu_4N][OsCl_4N]$. This feature is responsible for the very dark brown coloration of $[(Bu_4N)_7][\alpha_2\text{-}P_2W_{17}O_{61}\{Os^{VI}N\}]$.

^{183}W NMR spectroscopy of $[(Bu_4N)_4][\alpha\text{-}PW_{11}O_{39}\{Os^{VI}N\}]$: The ^{183}W spectrum of $[\alpha\text{-}PW_{11}O_{39}\{Os^{VI}N\}]^{4-}$ (contaminated with $[PW_{12}O_{40}]^{3-}$) has been already presented in a preliminary report.[35] The 12.5 MHz ^{31}P-decoupled spectrum of a purer sample is shown in Figure 1. As expected for C_s symmetry, it exhibits six narrow lines, with an (approximate) relative intensity ratio of 2:1:2:2:2:2. For the coupled spectrum all resonances are doublets with $^2J_{W,P}$ couplings of 1.2 to 1.5 Hz.

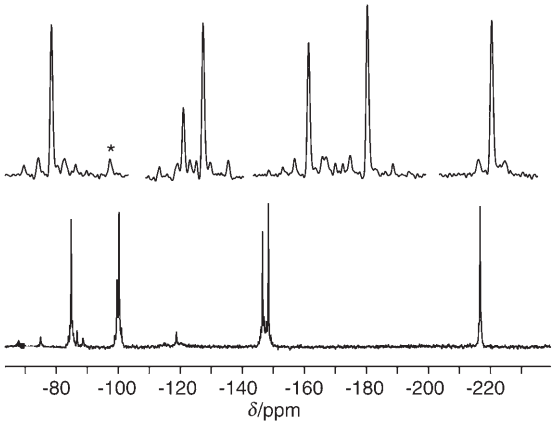

Figure 1. ^{183}W{^{31}P} NMR spectrum (12.5 MHz) of $[\alpha\text{-}PW_{11}O_{39}\{Os^{VI}N\}]^{4-}$ (1.27×10^{-1} mol L^{-1} in CD_3CN). Bottom: full spectrum; top: abscissa expansions of the individual signals showing the tungsten satellites. The resonance indicated by * originates from $[\alpha\text{-}PW_{12}O_{40}]^{3-}$.

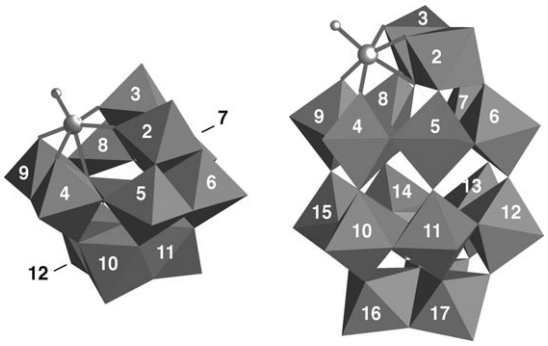

Figure 2. Postulated structures of $[\alpha\text{-}PW_{11}O_{39}\{Os^{VI}N\}]^{4-}$ (left) and $[\alpha_2\text{-}P_2W_{17}O_{61}\{Os^{VI}N\}]^{7-}$ (right) in polyhedral representations.

Table 1. Theoretical tungsten–tungsten connectivity matrix for $[\alpha\text{-}PW_{11}O_{39}\{Os^{VI}N\}]^{4-}$.[a,b]

Nucleus	2,3	4,9	5,8	6,7	10,12	11
2,3	δ		e	e		
4,9		δ	c		c	
5,8	e	c	δ	e	c	
6,7	e		e	δ		c
10,12		c	c		δ	e
11				c	e	δ

[a] The atom numbering (see Figure 2) is given according to IUPAC convention. [b] The off-diagonal entries are coupling constants: e = edge (small) couplings; c = corner (large) couplings.

Generally, assignment of the ^{183}W resonances to the structurally inequivalent W atoms can be done by using the homonuclear coupling constants $^2J_{W,W}$, which allows determination of the coupling partners and infers the W–W connectivity. Some conditions are required: 1) a nonambiguous starting point for the assignment, 2) the absence of degeneracy or signal overlaps, 3) the presence of well-resolved tungsten satellites, and 4) a sufficiently large distribution of the coupling-constant values. As a starting point, the line of intensity 1 ($\delta=-99.5$ ppm) is immediately assigned to the unique tungsten atom (W11) located in the vertical plane of symmetry, which also contains the osmium atom (see Figure 2). However, it is impossible to discriminate its tungsten satellites from those of the nearby 2W line at $\delta=-100.2$ ppm (Figure 1, top), and further assignment requires the use of homonuclear correlation spectroscopy (2D COSY). The theoretical connectivity matrix is displayed in Table 1.

Generally, corner couplings, that is, coupling between tungsten nuclei in corner-sharing octahedra (W-O-W angle ca. 150°), are in the range of 20 Hz, whereas edge couplings, that is, coupling between tungsten nuclei in edge-sharing octahedra (W-O-W angle ca. 120°), are significantly smaller (ca. 10 Hz). For lacunary species, a *trans* effect may cause some corner couplings to become larger than usual while others appear abnormally low,[49–52] but filling the lacuna with an addenda atom restores more or less normal values. Therefore, according to the theoretical connectivity matrix, eight correlations are expected: four strong ones, corresponding to corner couplings and four weak ones, for edge couplings. As seen in Figure 3, only six cross peaks are actually observed, corresponding to three strong and three weak couplings, respectively: the two missing correlations likely imply close resonances, that is, both around $\delta=-100$ and -147 ppm.

The correlation between the $\delta=-99.5$ (W11) and -84.7 ppm peaks with a J coupling of approximately 21 Hz leads to the assignment of the latter as W6(≡W7). The second correlation for the $\delta=-99.5$ ppm peak is not observed, which is likely because the expected cross peak falls near the diagonal; this leads to the assignment of the $\delta=-100.2$ ppm resonance to W10(≡W12). Starting from W6 ($\delta=-84.7$ ppm), we observe two correlations with the $\delta=-146.4$ and -216.6 ppm peaks, also mutually coupled; all these resonances are consistently assigned to the triad W2W5W6 (≡W3W8W7) with edge couplings of 10.6 Hz. As no other correlation is expected for W2(≡W3), while two supplementary ones should be observed for W5(≡W8), the $\delta=-216.6$ ppm peak corresponds to W2(≡W3) adjacent to the osmium atom, and the $\delta=-146.4$ ppm resonance is assigned to W5(≡W8). Finally, the remaining signal at $\delta=-148.3$ ppm is assigned to W4(≡W9) in the OsW_2 triad, corner-coupled to W10(≡W12). The missing correlation between W4 and W5 is again rationalized by the close chemical shifts of the coupling partners. With this assignment completed, reinvestigation of the high-resolution ^{31}P-decoupled 1D spectrum allows an analysis of the satellite patterns

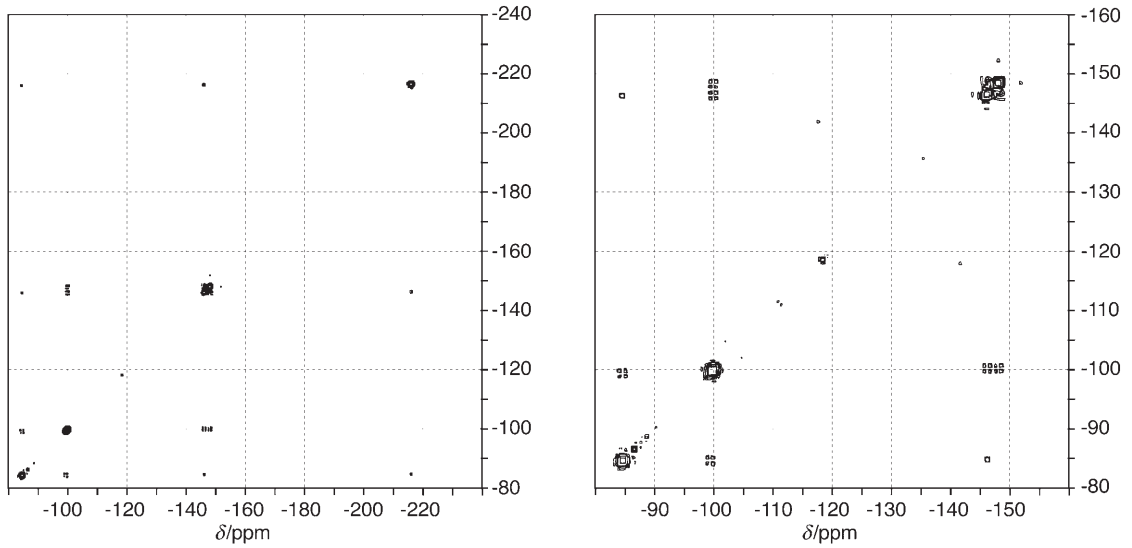

Figure 3. ^{183}W NMR 2D COSY spectrum (20.8 MHz) of $[\alpha\text{-}PW_{11}O_{39}\{Os^{VI}N\}]^{6-}$ (1.27×10^{-1} mol L^{-1} in CD_3CN). Left: full matrix; right: zoom of the region between $\delta=-80$ and -160 ppm.

(Figure 1, top) and the determination of all homonuclear coupling constants, including those related to AB systems. The resulting assignment is displayed in Table 2. As can be seen, the various coupling constants are all in the normal range, that is, 10 Hz for edge coupling and approximately 20 Hz for corner coupling, which implies that the osmium atom restores the regular geometry of the tungsten framework. Note also that the W2(≡W3) nuclei "corner-connected" to Os are shielded with respect to $[\alpha\text{-}PW_{12}O_{40}]^{3-}$ by 130 ppm. This agrees with previous observations made by Domaille who studied numerous monosubstituted Keggin anions: the most shielded tungsten nucleus is always that which is corner-connected to the addenda atom.[53]

Table 2. Experimental tungsten–tungsten connectivity matrix for $[\alpha\text{-}PW_{11}O_{39}\{Os^{VI}N\}]^{4-}$.[a]

Nucleus	2,3	4,9	5,8	6,7	10,12	11
2,3	−216.6		10.6	10.6		
4,9		−148.3	23.5 AB		20.2	
5,8	11.2	23.5 AB	−146.4	11.2	21	
6,7	10.6		10.6	−84.7		20.8 AB
10,12		20.5	20.5		−100.2	10 AB
11				20.5 AB	10 AB	−99.5

[a] On-diagonal entries are chemical shifts [ppm]; off-diagonal entries are coupling constants [Hz].

^{183}W NMR spectroscopy of $[(Bu_4N)_3][\alpha\text{-}PW_{11}O_{39}\{Re^{VII}N\}]$: Six lines are expected in the ^{183}W NMR spectrum of $[\alpha\text{-}PW_{11}O_{39}\{Re^{VII}N\}]^{3-}$, as found for the previous monosubstituted Keggin anion $[\alpha\text{-}PW_{11}O_{39}\{Os^{VI}N\}]^{4-}$ and according to the C_s symmetry. Actually, only five resonances are observed, with an (approximate) relative intensity ratio of 2:4:2:2:1 ($\delta=-55.5$ (2W), −83.6 (4W), −84.2 (2W), −87.5 (2W), −92.4 ppm (1W); see Figure 4); this indicates that, due to the narrow chemical-shift dispersion ($\Delta\delta=37$ ppm), two resonances are accidentally degenerate, and the spectrum may be effectively reconciled with C_s symmetry. The small ^{183}W chemical-shift variation for $[\alpha\text{-}PW_{11}O_{39}\{Re^{VII}N\}]^{3-}$ contrasts with $[\alpha\text{-}PW_{11}O_{39}\{Os^{VI}N\}]^{4-}$ ($\Delta\delta=132$ ppm) and, more generally, for all monosubstituted Keggin anions incorporating d^n metal cations for which the ^{183}W chemical-shift range amounts to more than 100 ppm.[54,55] Actually, it has already been noticed that substitution of a d^0 configuration cation (V^{5+}, Mo^{6+}) for W^{6+} in a polyoxotungstate framework induces relatively small ^{183}W NMR chemical-shift variations, usually in the range of 50 ppm for V and of 10 ppm for Mo.[21,53,56–58]

^{183}W NMR spectroscopy of $[(Bu_4N)_7][\alpha_2\text{-}P_2W_{17}O_{61}\{Os^{VI}N\}]$: The spectrum of $[\alpha_2\text{-}P_2W_{17}O_{61}\{Os^{VI}N\}]^{7-}$ exhibits the nine lines, labeled A to I in the order of decreasing frequency, with a relative (approximate) intensity ratio of 2:2:1:2:2:2:2:2:2 expected for C_s symmetry (see Figure 5). The theoretical connectivity matrix is shown

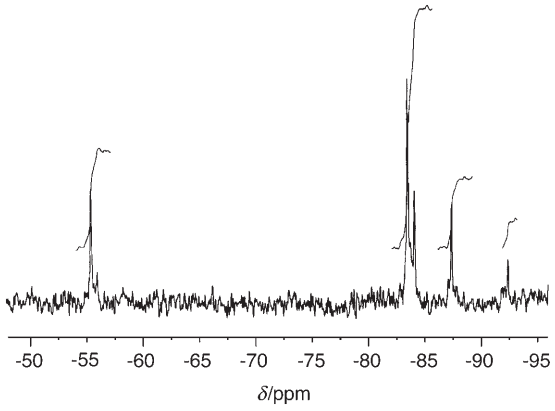

Figure 4. ^{183}W NMR spectrum (20.8 MHz) of $[\alpha\text{-}PW_{11}O_{39}\{Re^{VII}N\}]^{3-}$ (1.46×10^{-2} mol L^{-1} in CH_3CN/CD_3COCD_3).

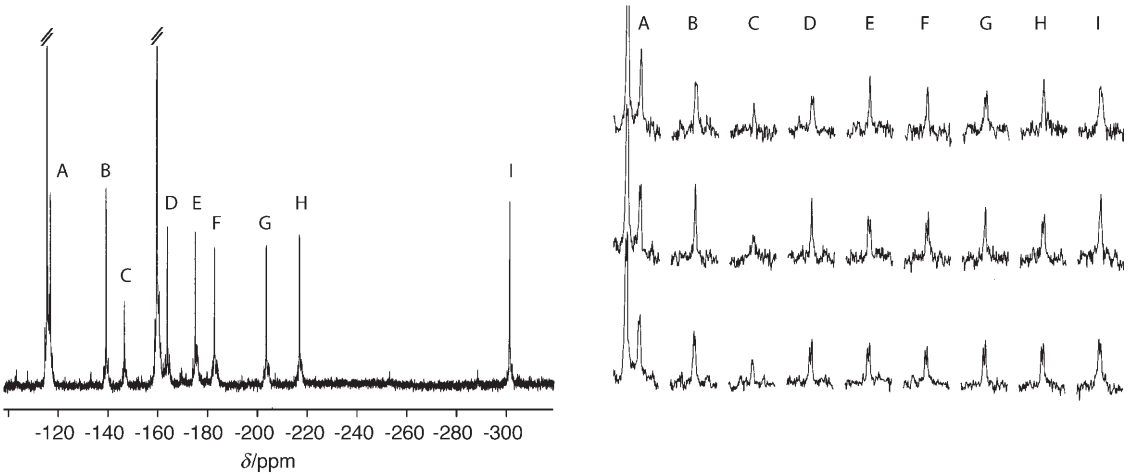

Figure 5. Left: ^{183}W NMR spectrum (12.5 MHz) of $[\alpha_2$-$P_2W_{17}O_{61}\{Os^{VI}N\}]^{7-}$ (ca. 2.64 10^{-2} mol L^{-1} in DMF/CD_3COCD_3). The intense signals from $[\alpha$-$P_2W_{18}O_{62}]^{6-}$ present as a major impurity are truncated. Right: abscissa expansion of the individual lines for different ^{31}P-decoupling conditions; bottom, no decoupling; middle, CW ^{31}P irradiation at $\delta = -11.4$ ppm (PW_8Os); top, CW ^{31}P irradiation at $\delta = -12.6$ ppm (PW_9).

in Table 3 with no distinction between the two types of corner couplings, that is, intergroup (between dyad and/or triads) and interbelt couplings expected in the range of 20 and 30 Hz, respectively.

Table 3. Theoretical tungsten–tungsten connectivity matrix for $[\alpha_2$-$P_2W_{17}O_{61}\{Os^{VI}N\}]^{7-}$.[a,b]

Nucleus	2,3	4,9	5,8	6,7	10,15	11,14	12,13	16	17,18	Subunit	Type
2,3	δ		c	c						PW_8Os	cap
4,9		δ	e		c					PW_8Os	belt
5,8	c	e	δ	c		c				PW_8Os	belt
6,7	c		c	δ			c			PW_8Os	belt
10,15		c			δ	e		c		PW_9	belt
11,14			c		e	δ	c		c	PW_9	belt
12,13				c		c	δ		c	PW_9	belt
16					c			δ	e	PW_9	cap
17,18						c	c	e	δ	PW_9	cap

[a] The atom numbering (see Figure 2) is given according to the IUPAC convention. [b] The off-diagonal entries are coupling constants: e = edge (small) couplings, c = corner (large) couplings.

The line C ($\delta = -146$ ppm), with intensity 1 was immediately assigned to the tungsten atom located in the unique position in the vertical plane of symmetry, which also contains the osmium atom (W16, see Figure 2). Further assignment can be made by means of selective ^{31}P-decoupling experiments (Figure 5, right). Actually, with continuous wave (CW) low-power irradiation at the resonance frequency of the most shielded ^{31}P atom ($\delta = -12.61$ ppm), five ^{183}W resonances, namely, A ($\delta = -116.5$ ppm), C ($\delta = -146.0$ ppm), E ($\delta = -174.4$ ppm), F ($\delta = -182.3$ ppm), and H ($\delta = -216.0$ ppm), become singlets, instead of doublets without decoupling (under high-resolution conditions). All these lines (^{183}W and ^{31}P) must therefore be assigned to the PW_9 subunit. In the second selective decoupling experiment, the four remaining ^{183}W resonances B ($\delta = -139.0$ ppm), D ($\delta = -163.2$ ppm), G ($\delta = -202.9$ ppm), and I ($\delta = -300.9$ ppm) become singlets, in agreement with their assignment to the four inequivalent tungsten atoms of the PW_8OsN subunit (see Table 4).

Further steps in the assignment may be done with the help of the $^2J_{W,P}$ coupling constants, which, in saturated species, discriminate between cap ($^2J_{W,P} \leq 1.2$ Hz) and belt ($^2J_{W,P} > 1.2$ Hz) sites. The three high-frequency lines, A, B, and C, all with $^2J_{W,P}$ of approximately 1 Hz, can then be assigned to tungsten atoms W2(≡W3), W17(≡W18), and W16, respectively.

Before continuing, we note the chemical-shift variations of the cap resonances with respect to that of $[\alpha$-$P_2W_{18}O_{62}]^{6-}$ present as an impurity. It appears that all nuclei are shielded, with the most-affected (W16, $\Delta\delta = -30.4$ ppm) and least-affected

Table 4. Comparison of the ^{183}W NMR data of solutions of $[\alpha_2$-$P_2W_{17}O_{61}$-$\{Os^{VI}N\}]^{7-}$ and $[\alpha$-$P_2W_{18}O_{62}]^{6-}$ as a $[Bu_4N]^+$ salt in DMF/CD_3COCD_3.[a]

$[\alpha$-$P_2W_{18}O_{62}]^{6-}$	$[\alpha_2$-$P_2W_{17}O_{61}\{Os^{VI}N\}]^{7-}$				
	PW_9	$\Delta\delta$	PW_8Os	$\Delta\delta$	Nucleus
−115.6 (cap)	−116.5	−0.9			17,18
			−139.0	−23.4	2,3
	−146.0	−30.4			16
−159.6 (belt)			−163.2	−3.6	6,7
	−174.4	−14.8			12,13
	−182.3	−22.7			11,14
			−202.9	−43.3	5,8
	−216.0	−56.4			10,15
			−300.9	−141.3	4,9

[a] Chemical shifts (δ) [ppm]; $\Delta\delta = \delta(P_2W_{17}OsN) - \delta(P_2W_{18})$.

nuclei (W17(≡W18), $\Delta\delta \approx 0$ ppm) belonging to the trimetallic group on the opposite side to the osmium atom.

The twelve tungsten nuclei of the two belts are also shielded with respect to $[\alpha\text{-}P_2W_{18}O_{62}]^{6-}$. Both the less-shielded nuclei D ($\Delta\delta = -3.6$ ppm) and the more-shielded nuclei I ($\Delta\delta = -141.3$ ppm) belong to the PW_8Os unit. By analogy with $[\alpha\text{-}PW_{11}O_{39}\{Os^{VI}N\}]^{4-}$ (see above), the more-shifted signal can be assigned to W4(≡W9) corner-connected to the osmium atom. On the contrary, the tungsten W2(≡W3) edge-connected to the osmium atom in the cap resonates closer to $[\alpha\text{-}P_2W_{18}O_{62}]^{6-}$ ($\Delta\delta = -23.4$ ppm). This may be the result of two opposing effects: shielding experienced by all tungsten atoms likely due to an anionic charge increase, which is counterbalanced by a deshielding effect for a tungsten edge-connected to the perturbed atom.[53] Note that the shielding effect is expected to decrease with increasing tungsten–osmium distance, because the influence of the supplementary negative charge should probably vanish.

Assignment of the PW_9 belt requires either correlation spectroscopy or determination of the connectivity through observation of the coupling constants. However the low concentration (less than 3×10^{-2} M) precludes any 2D experiment and the signal-to-noise ratio for the 1D spectrum remains too low to observe all tungsten satellites. Alternatively, it may be helpful to use the method proposed by Pope and Sveshnikov, based on peak height.[59]

As W2(≡W3), W4(≡W9), W16, and W17(≡W18) have already been assigned, W5(≡W8), and W6(≡W7) for the PW_8Os group and W10(≡W15), W11(≡W14), and W12(≡W13) for the PW_9 belt remain.

For the PW_8Os belt, the height of the three lines is in the order I > D > G. According to the theoretical connectivity matrix, they are then consistently assigned to W4(≡W9) (two couplings), W6(≡W7) (three couplings), and W5(≡W8) (four couplings), respectively. For the PW_9 belt, line F is smaller than the two other ones. It may be assigned to W11(≡W14) (four couplings). The two last signals (E and H) have equal height in agreement with the same number of couplings (three). E presents satellites with an AB pattern, which leads to its assignment as W12(≡W13) corner-coupled to W11(≡W14) at the close $\delta = -182.3$ ppm. Consequently, line H corresponds to W10(≡W15). All these data are summarized in Table 4.

It appears then that, with respect to the Dawson $[\alpha\text{-}P_2W_{18}O_{62}]^{6-}$ anion, the most shielded ^{183}W nuclei are, in decreasing order, W4(≡W9), W10(≡W15), W5(≡W8), and W16. Except for W5(≡W8), they correspond to tungsten atoms mutually in *trans* positions when starting from the osmium addendum atom, and which are removed in the hexavacant $[H_2P_2W_{12}O_{48}]^{12-}$.

^{183}W NMR spectroscopy of $[(Bu_4N)_7][\alpha_1\text{-}P_2W_{17}O_{61}\{Os^{VI}N\}]$: Seventeen lines are expected in the ^{183}W NMR spectrum of the unsymmetrical chiral anion $[\alpha_1\text{-}P_2W_{17}O_{61}\{Os^{VI}N\}]^{7-}$. As for the α_2 isomer, the various samples were always contaminated by the nonsubstituted highly symmetrical anion $[\alpha\text{-}P_2W_{18}O_{62}]^{6-}$. The amount of this impurity, as shown by ^{31}P NMR spectroscopy, may drop to 10–15%; even with such a low concentration, the two ^{183}W NMR resonances of $[\alpha\text{-}P_2W_{18}O_{62}]^{6-}$ nevertheless remain of comparable intensity and even larger than each individual $[\alpha_1\text{-}P_2W_{17}O_{61}\{Os^{VI}N\}]^{7-}$ signal. The 12.5 MHz spectrum of a solution of $[\alpha_1\text{-}P_2W_{17}O_{61}\{Os^{VI}N\}]^{7-}$ in acetonitrile with less than 15% $[\alpha\text{-}P_2W_{18}O_{62}]^{6-}$ is presented in Figure 6. Only eleven isolated signals of the same integrated intensity are effectively identified at $\delta = -102.3$, -106.8, -132.1, -157.2, -161.4, -168.3, -178.6, -192.7 -206.2, -252.0, and -287.2 ppm. Except for very small signals from the α_2 isomer, the spectrum also presents a single line at the chemical shift of $[\alpha\text{-}P_2W_{18}O_{62}]^{6-}$ ($\delta = -115.3$ ppm, intensity ca. 2) and two strongly overlapping multiplets around $\delta = -160$ and -174.4 ppm (with intensities ca. 4 and 3, respectively). The six missing signals of $[\alpha_1\text{-}P_2W_{17}O_{61}\{Os^{VI}N\}]^{7-}$ are likely partially degenerated and contribute to these three resonances along with the two signals of $[\alpha\text{-}P_2W_{18}O_{62}]^{6-}$. No assignment can be performed except for the two low-frequency signals at $\delta = -252.0$ and -287.2 ppm, which likely correspond to the two tungsten nuclei in the belt corner-connected to the osmium addendum atom.

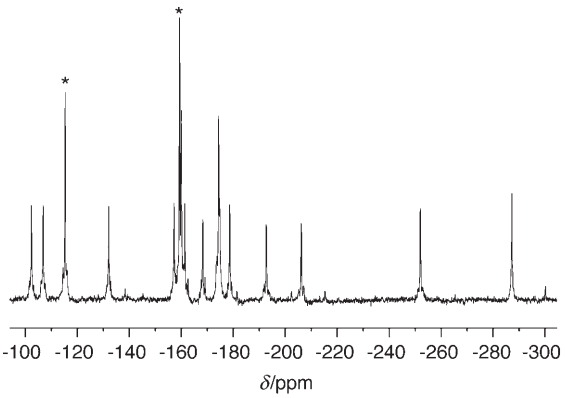

Figure 6. ^{183}W NMR spectrum (20.8 MHz) of $[\alpha_1\text{-}P_2W_{17}O_{61}\{Os^{VI}N\}]^{7-}$ (ca. 7×10^{-2} mol L^{-1} in CH_3CN/CD_3CN). The resonances indicated by * are due to $[\alpha\text{-}P_2W_{18}O_{62}]^{6-}$.

^{15}N NMR spectroscopy of $[(Bu_4N)_4][\alpha\text{-}PW_{11}O_{39}\{Os^{15}N\}]$, $[(Bu_4N)_7][\alpha_2\text{-}P_2W_{17}O_{61}\{Os^{15}N\}]$, and $[(Bu_4N)_7][\alpha_1\text{-}P_2W_{17}O_{61}\{Os^{15}N\}]$: The signals of $[\alpha\text{-}PW_{11}O_{39}\{Os^{15}N\}]^{4-}$ and $[\alpha_2\text{-}P_2W_{17}O_{61}\{Os^{15}N\}]^{7-}$ are observed at the same chemical shift ($\delta = 421.8$ and 421.6 ppm, respectively), whereas that of $[\alpha_1\text{-}P_2W_{17}O_{61}\{Os^{15}N\}]^{7-}$ is shifted to a higher frequency ($\delta = 441.6$ ppm), nearly at the same position as that of the $[OsCl_4N]^-$ precursor ($\delta = 446.4$ ppm). The shift between cap and belt nitrido ligands ($\Delta\delta(^{15}N) = 20$ ppm) is similar to that observed by ^{17}O NMR spectroscopy for the terminal oxo groups of $[\alpha\text{-}P_2W_{18}O_{62}]^{6-}$ ($\delta_{cap} = 739$ ppm; $\delta_{belt} = 759$ ppm).[60]

EPR spectroscopy of $[(Bu_4N)_4][\alpha\text{-}PW_{11}O_{39}\{Re^{VI}N\}]$: The experimental frozen-solution and powder spectra of $[(Bu_4N)_4][\alpha\text{-}PW_{11}O_{39}\{Re^{VI}N\}]$, registered at conventional (X-band,

9.3 GHz) and high (190 GHz) frequencies, are shown in Figure 7a and b, respectively. The 190 GHz spectrum, owing to the overwhelming electronic Zeeman term, is much simpler.

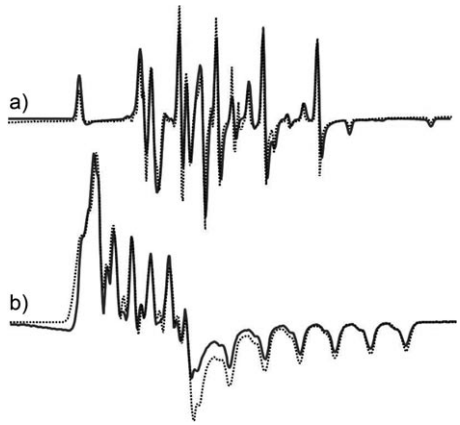

Figure 7. Experimental (gray line) and simulated (dotted line) X-band as a frozen solution at 90 K (a) and 190 GHz as a powder at 5 K (b) EPR spectra of $[(Bu_4N)_4][\alpha\text{-}PW_{11}O_{39}\{Re^{VI}N\}]$.

It is dominated by two sets of six hyperfine lines that are well separated into a "parallel" and a "perpendicular" region that arise from the interaction of the unpaired electron with nuclear spin $I=5/2$ of both rhenium isotopes, ^{187}Re ($g_n=1.2879$, natural abundance $=62.6\,\%$) and ^{185}Re ($g_n=1.2748$, natural abundance $=37.4\,\%$) in which g_n is the Lande nuclear factor. There is also a strong shift of the g tensor components below the spin-only value. Similar to other $[L_n\{Re^{VI}N\}]$ complexes,[39] no traces of the nitrogen superhyperfine structure were detected. A closer inspection of the "perpendicular" part of the spectrum reveals small anisotropies of the x and y components. Because the two Re isotopes have very similar nuclear magnetic moments, their isotope hyperfine splitting could not be resolved at the observed line widths. Yet, besides the main signal, one additional weak component could be detected near each of the principal "parallel" hyperfine lines in the 190 GHz spectrum (Figure 7b). The intensity of this signal is too low in comparison with that expected from the natural abundance of both isotopes, and it is not seen at 9.3 GHz; it can therefore not be assigned to the ^{185}Re isotopomer. Because of slightly different g values, a more likely assignment is to a minor closely related $\{Re^{VI}N\}$ species with slightly different parameters.

The major feature of the frozen-solution X-band spectrum is an extremely large anisotropic rhenium hyperfine splitting with very uneven spacings of the primary lines. However, in contrast to frozen-solution spectra of $[(Bu_4N)_6][\alpha_2\text{-}P_2W_{17}O_{61}\{Re^{VI}O\}]$ of the Dawson structure reported earlier,[61] no significant changes in the line widths were observed. This lack of change indicated that the effects attributable to random strain or structural distortions are much smaller in our case. Although some of the "parallel" (z) hyperfine bands can be readily assigned by comparison to the 190 GHz spectrum, the prevailing "perpendicular" (x and y) features are mixed with weaker lines. These weaker lines are assigned to "forbidden" secondary ($\Delta m_I=\pm1$) and tertiary ($\Delta m_I=\pm2$) transitions, induced by strong mixing of the nuclear and electronic states that are of comparable energy at the X-band level.[62,63] The intensities of those transitions have nonzero values in the range $0<\theta<90°$, so they appear between the allowed transitions ($\Delta m_S=\pm1$, $\Delta m_I=0$), and become important when the quadrupole interaction is greater than $\approx{}^1/_{10}$ of the metal hyperfine interaction. The positions of the allowed transitions are not very suitable for determining the quadrupole parameters, and secondary and tertiary lines provide a better means of their reliable quantization.

The resultant spin Hamiltonian describing the EPR spectra may be written as shown in Equation (1):

$$\mathscr{H}=\beta_e\mathbf{S}\cdot\boldsymbol{g}\cdot\boldsymbol{B}+\mathbf{S}\cdot\boldsymbol{A}\cdot\mathbf{I}-\beta_n g_n\mathbf{I}\cdot\boldsymbol{B}+\mathbf{I}\cdot\boldsymbol{P}\cdot\mathbf{I} \quad (1)$$

in which β_e and β_n are the electron and nuclear Bohr magnetons, respectively, **S** and **I** are the electron and nuclear spin-operator vectors, and ***B*** represents the magnetic field. The first term describes the electron Zeeman interaction gauged by the ***g*** tensor; the second term is the electron-spin–nuclear-spin hyperfine interaction (tensor ***A***). The last two terms account for nuclear Zeeman and quadrupole interactions (tensor ***P***). Computer simulations of the spectra were performed by using an exact diagonalization of the spin-Hamiltonian matrix.

The C_s symmetry of the $[(Bu_4N)_4][\alpha\text{-}PW_{11}O_{39}\{Re^{VI}N\}]$ paramagnet implies a monoclinic EPR spectrum; however, the x–y anisotropy ($g_{xx}-g_{yy}$ and $A_{xx}-A_{yy}$) and the noncoincidence between the ***g*** and ***A*** tensor principal axes were found to be rather small ($\beta=4\pm1$) in comparison with those of $[(Bu_4N)_6][\alpha_2\text{-}P_2W_{17}O_{61}\{Re^{VI}O\}]$ ($\beta=15°$).[61] Figure 7a shows the experimental 9.3 GHz spectrum along with the best-fit simulation. The following spin-Hamiltonian parameters were obtained: $g_x=1.910(3)$, $g_y=1.894(1)$, $g_z=1.779(2)$, $|A_x|=1248(4)$ MHz, $|A_y|=1208(5)$ MHz, $|A_z|=2382(8)$ MHz, $|P_x|=48(6)$ MHz, $|P_y|=42(6)$ MHz, $|P_z|=91(5)$ MHz, $\beta_A=3\pm1°$, with the principal axes of ***A*** and ***P*** nearly coincident. In order to determine the absolute signs of the principal values of the quadrupole tensor, one must know the absolute signs of the principal values of the hyperfine tensor. From the solution spectra of $[(Bu_4N)_4][\alpha\text{-}PW_{11}O_{39}\{Re^{VI}N\}]$ we found $|A_{av}|\approx1590$ MHz, thus all three principal values of the ***A*** tensor have to exhibit the same sign.

In view of the noncoincidence of the ***g*** and ***A*** principal axes, molecular analysis of the spin-Hamiltonian parameters can be performed within the C_s symmetry.[36] The nearest environment of the rhenium ion is a distorted octahedron constituted by four oxygen atoms at a distance of 1.9 Å, a more distal axial oxygen atom at 2.4 Å, and a terminal nitrogen atom at 1.6 Å. By following a procedure by Nilges et al.,[61] we defined a coordinate system with the z (directed along the terminal Re–N bond) and y axes lying in the symmetry plane, with the x axis being normal and bisecting the O–Re–O bonds. Taking into account that the Re–N bond

strongly dominates the ligand field, the $\boldsymbol{g}$, $\boldsymbol{A}$, and $\boldsymbol{P}$ tensors exhibit nearly 'axial' values with $g_z \gg g_x \approx g_y$, $A_z \gg A_x \approx A_y$ and $P_z \gg P_x \approx P_y$, which implies a ground state singly occupied molecular orbital (SOMO) composed mainly of $d_{x^2-y^2}$ with small admixtures of d_{yz} and d_{z^2}, allowed by the C_s symmetry. Indeed, because the nitrogen superhyperfine splitting was not resolved, no lobe of the SOMO should be directed toward the nitrogen ligand, thus any contribution of d_{yz} and d_{z^2} to the SOMO should be rather small. In such a case, the largest g_z and A_z components are directed approximately (within a few degrees) along the Re–N bond.

The Re hyperfine tensor can be expressed in terms of isotropic and anisotropic contributions as shown in Equation (2):

$$\boldsymbol{A} = a_{iso}\mathbf{E} + \boldsymbol{T} \qquad (2)$$

in which a_{iso} represents the Fermi contact term, $\mathbf{E}$ is the unit matrix, and $\boldsymbol{T}$ is the dipolar term. As usual we assume that $a_{iso} = <\boldsymbol{A}> = {}^1/_3(A_x + A_y + A_z)$. The values of a_{iso} and $\boldsymbol{T}$ can next be used to determine the coefficients of s and d orbitals in the SOMO. Neglecting the contribution due to the spin–orbit coupling, at the first approximation, the resultant hyperfine tensor of rhenium can be decomposed in the following way:

$$\boldsymbol{A}/h = \begin{vmatrix} -1248 & & \\ & -1208 & \\ & & -2382 \end{vmatrix} = -1613 + \begin{vmatrix} 391 & & \\ & 391 & \\ & & -782 \end{vmatrix} + \begin{vmatrix} -26 & & \\ & 13 & \\ & & 13 \end{vmatrix}$$

in which $\boldsymbol{A}/h$ is in MHz and h is Planck's constant. Spin-orbit coupling perturbs these results, adding terms to the diagonal matrix components on the order of $P(g_{ii} - g_e)$.[64] Elucidation of this problem, along with detailed analysis of the quadrupole effects, will be the subject of another paper.

By applying the generally accepted formalism,[65] the spin-density repartition (c^2) over the 6s and 5d orbitals can be obtained from the simple formula $c_s^2 \approx a_{iso}^{Re}/A_0^{Re}$ and $c_d^2 \approx B^{Re}/B_0^{Re}$, where $A_0^{Re} = 35490$ MHz is the atomic isotropic hyperfine constant and $B_0^{Re} = 462.8$ MHz is the atomic dipolar hyperfine constant for ^{187}Re. The negative value of a_{iso} is consistent with the fact that spin polarization dominates over the direct contribution of the $|6s>$ orbital to the SOMO, so it cannot reliably be assessed. For estimation of both 5d coefficients, we obtain $c^2(d_{x^2-y^2}) = a^2 = 391$ MHz/462.8 MHz = 0.85 and $c^2(d_{yz}) = b^2 = 13$ MHz/462.8 MHz = 0.029. The remaining part is distributed over $5d_{z^2}$ (c^2) and the ligands. These values are in agreement with those previously found for other transition-metal ions such as W, Mo, or V hosted in Keggin structures.[66]

The observed $\boldsymbol{g}$ tensor is in full accordance with the results of the hyperfine structure analysis. Taking into account that $d_{x^2-y^2}$ dominates in the SOMO, thus, the minor quadratic terms can be ignored, we obtain the experimentally observed sequence $g_{zz} \approx g_e - 8\lambda_{Re}a^2/(E_{xy} - E_{x^2-y^2}) < g_{yy} \approx g_e - 2a\lambda_{Re}(a - \sqrt{3}c)/(E_{xz} - E_{x^2-y^2})$, $g_{xx} \approx g_e - 2a\lambda_{Re}(a + \sqrt{3}c)/(E_{yz} - E_{x^2-y^2})$ for $c < 0$.[61] For the observed $c_{yz}/c_{x^2-y^2}$ hybridization ratio, the noncoincidence angle β_A between the $\boldsymbol{A}$ and $\boldsymbol{g}$ tensors differs by only approximately 1°, again in good agreement with the simulation results.

To summarize, the EPR data show that the odd electron in $[(Bu_4N)_4][\alpha\text{-}PW_{11}O_{39}\{Re^{VI}N\}]$ is primarily localized on the rhenium $5d_{x^2-y^2}(d_\pi)$ orbital overlapping with $2p_\pi$ orbitals of the in-plane oxygen ligands. The high-valence Re metal center exhibits C_s symmetry, and can be stabilized within the Keggin framework. The weak m_I dependence of the line widths indicates a well-ordered local surrounding of the nitrido-rhenium magnetophore.

Cyclic voltammetry of $[(Bu_4N)_4][\alpha\text{-}PW_{11}O_{39}\{Re^{VI}N\}]$: Four reversible waves at +0.51, −0.46, −1.43, and −1.88 V versus SCE and one irreversible wave at −2.56 V are observed in the voltammogram of $[(Bu_4N)_4][\alpha\text{-}PW_{11}O_{39}\{Re^{VI}N\}]$ recorded in acetonitrile at a carbon electrode (see Figure 8 and Table 5). The four former waves correspond to one-electron processes, which are attributed, respectively, to the oxidation of Re^{VI} to Re^{VII} and to the successive reductions of Re^{VI} to Re^{V}, Re^{IV}, and Re^{III}.[36] The latter wave is a multielectron process owing to the reduction of the polyoxotungstate framework. Interestingly, the relatively low oxidation potential of $[(Bu_4N)_4][\alpha\text{-}PW_{11}O_{39}\{Re^{VI}N\}]$ (0.51 V) suggests that $[(Bu_4N)_3][\alpha\text{-}PW_{11}O_{39}\{Re^{VII}N\}]$ can be prepared easily. Indeed, it has been synthesized by oxidation of $[(Bu_4N)_4][\alpha\text{-}PW_{11}O_{39}\{Re^{VI}N\}]$ by $(Bu_4N)Br_3$.[35]

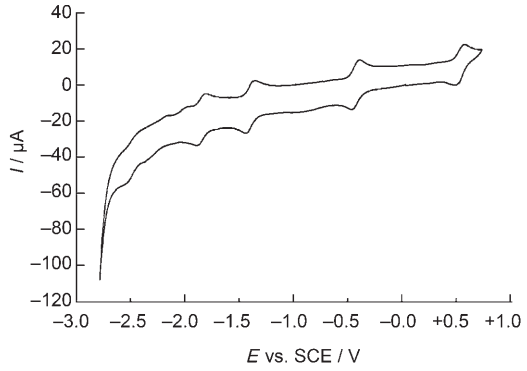

Figure 8. Cyclic voltammogram of $[(Bu_4N)_4][\alpha\text{-}PW_{11}O_{39}\{Re^{VI}N\}]$ (1 mmol L^{-1} in CH_3CN, 0.1 mol L^{-1} $(Bu_4N)BF_4$, E vs. SCE [V] at a carbon electrode, 100 mV s^{-1}).

Table 5. Electrochemical data (in V) versus SCE recorded on a CH_3CN sample of $[(Bu_4N)_4][\alpha\text{-}PW_{11}O_{39}\{Re^{VI}N\}]$.

	Re^{6+}/Re^{7+}	Re^{6+}/Re^{5+}	Re^{5+}/Re^{4+}	Re^{4+}/Re^{3+}
E_{pa}	0.54	−0.42	−1.39	−1.83
E_{pc}	0.47	−0.49	−1.46	−1.92
${}^1/_2(E_{pa}+E_{pc})$	0.51	−0.46	−1.43	−1.88
$E_{pa}-E_{pc}$	0.07	0.07	0.07	0.09

ESI mass spectrometry of $[(Bu_4N)_4][\alpha\text{-}PW_{11}O_{39}\{Os^{VI}N\}]$ and $[(Bu_4N)_4][\alpha\text{-}PW_{11}O_{39}\{Re^{VI}N\}]$: The ESI mass spectrum of $[(Bu_4N)_4][\alpha\text{-}PW_{11}O_{39}\{Re^{VI}N\}]$ displays a base peak centered at m/z 960 and another isotopic cluster at m/z 1559 (5%) (see Figure 9). These quasi-molecular species are characterized by a $\Delta(m/z) = {}^1/_3$ and ${}^1/_2$ Thomson increment, which implies triply and doubly charged species, respectively. The signal at m/z 1559 is thus assigned to the $[Bu_4N][\alpha\text{-}HPW_{11}O_{39}\{Re^{VI}N\}]^{2-}$ aggregate, whereas the signal at m/z 960 is attributed to $[\alpha\text{-}HPW_{11}O_{39}\{Re^{VI}N\}]^{3-}$. Aggregates between POMs and $[Bu_4N]^+$ ions are precedented in the literature and have been observed, for example, with the $[Bu_4N]^+$ salts of $[\alpha_2\text{-}P_2W_{17}O_{61}\{Re^{VI}O\}]^{6-}$,[61] $[\alpha\text{-}PW_{11}O_{39}\{Re^{V}NPh\}]^{4-}$,[22] and $[\alpha\text{-}PW_{11}O_{39}\{Mo^{V}O\}]^{4-}$.[21]

The ESI mass spectrum of $[(Bu_4N)_4][\alpha\text{-}PW_{11}O_{39}\{Os^{VI}N\}]$ displays a base peak centered at m/z 1442 characterized by a $\Delta(m/z) = {}^1/_2$ Thomson increment (see Figure 9), and was attributed to $[\alpha\text{-}H_2PW_{11}O_{39}\{Os^{VI}N\}]^{2-}$.

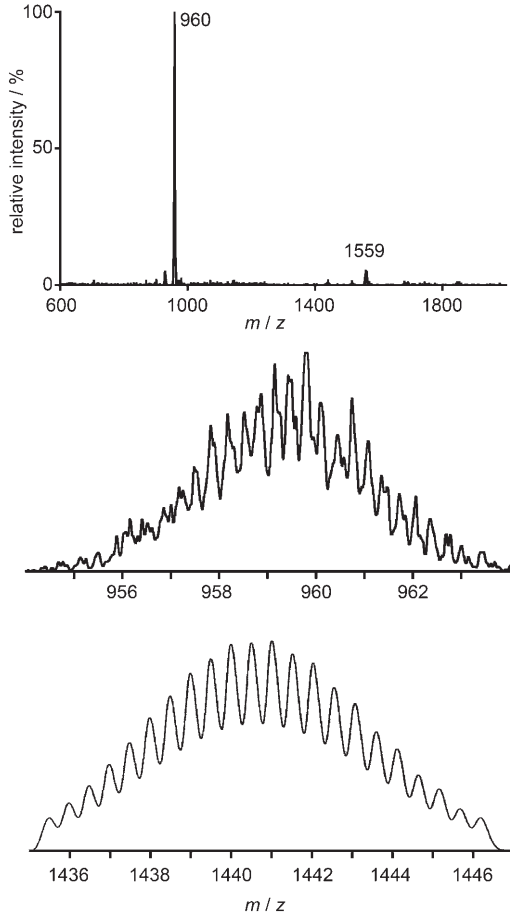

Figure 9. ESI spectra of $[(Bu_4N)_4][\alpha\text{-}PW_{11}O_{39}\{Re^{VI}N\}]$ (top) and enlargement of the base peaks of $[(Bu_4N)_4][\alpha\text{-}PW_{11}O_{39}\{Re^{VI}N\}]$ (middle) and $[(Bu_4N)_4][\alpha\text{-}PW_{11}O_{39}\{Os^{VI}N\}]$ (bottom).

Conclusion

In this paper, the synthesis of $[\alpha_2\text{-}P_2W_{17}O_{61}\{Os^{VI}N\}]^{7-}$ and $[\alpha_1\text{-}P_2W_{17}O_{61}\{Os^{VI}N\}]^{7-}$ as tetrabutylammonium salts are described for the first time. We also present two alternative routes to the synthesis of $[(Bu_4N)_4][\alpha\text{-}PW_{11}O_{39}\{Re^{VI}N\}]$ that we have previously reported.[35] Several methods including ^{183}W and ^{15}N NMR, EPR, IR, and UV-visible spectroscopies, electrochemistry, and ESI mass spectrometry have been used to characterize $[\alpha_2\text{-}P_2W_{17}O_{61}\{Os^{VI}N\}]^{7-}$, $[\alpha_1\text{-}P_2W_{17}O_{61}\{Os^{VI}N\}]^{7-}$, $[\alpha\text{-}PW_{11}O_{39}\{Re^{VI}N\}]^{4-}$, and $[\alpha\text{-}PW_{11}O_{39}\{Os^{VI}N\}]^{4-}$ thoroughly. Work in progress includes nitrogen-atom transfer reactions from nitrido derivatives and synthesizing other nitrogenous heteropolyanion derivatives, such as organoimido and phosphorane iminato species.

Experimental Section

Materials: $K_{10}[\alpha_2\text{-}P_2W_{17}O_{61}]$, $K_{10}[\alpha_1\text{-}P_2W_{17}O_{61}]$,[67] $[(Bu_4N)_4][\alpha\text{-}H_3PW_{11}O_{39}]$,[68] $[Bu_4N][OsCl_4N]$,[69] and $[Bu_4N][ReCl_4N]$[39] were prepared as described in the literature. $[ReCl_3(N_2Ph_2)(PPh_3)_2]$ was obtained by using a slight modification to the procedure described by Dilworth et al.:[40] 5.7 equiv of *N*,*N*-diphenylhydrazinium chloride were used and the reaction time was extended to 5 h. Tetrabutylammonium tetrafluoroborate was synthesized from commercial (Aldrich) sodium tetrafluoroborate and tetrabutylammonium hydrogen sulfate and was dried overnight at 60°C. Triethylamine was purchased from Aldrich and stored on sodium wire. Reagent-grade acetonitrile was dried over calcium hydride before distillation. Reagent-grade diethyl ether and methanol were used as received.

Preparation of $[(Bu_4N)_7][\alpha_2\text{-}P_2W_{17}O_{61}\{Os^{VI}N\}]$: $[Bu_4N][OsCl_4N]$ (0.120 g, 0.204 mmol) in methanol (5 mL) was added to a suspension of $K_{10}[\alpha_2\text{-}P_2W_{17}O_{61}]$ (0.904 g, 0.198 mmol) in distilled water (25 mL). The reaction turned very dark brown immediately. After 19 h at room temperature, $(Bu_4N)Br$ (0.402 g, 1.250 mmol) in distilled water (50 mL), acetonitrile (25 mL), and dichloromethane (10 mL) was added. The organic layer was separated (additional CH_2Cl_2 may be required to completely separate the phases), dried over K_2CO_3, the solvents were removed in vacuo, and the product was washed once with diethyl ether. Yield: 0.931 g (74%). This black solid was found to be $[(Bu_4N)_7][\alpha_2\text{-}P_2W_{17}O_{61}\{Os^{VI}N\}]$ contaminated with approximately 4.5% of $[(Bu_4N)_6][\alpha\text{-}P_2W_{18}O_{62}]$ as judged by using ^{31}P NMR spectroscopy ($\delta = -11.9$ ppm). The material can be recrystallized from acetonitrile/diethyl ether. ^{31}P NMR (CD_3CN): $\delta = -11.4$, -12.6 ppm; ^{15}N NMR (DMF/CD_3COCD_3): $\delta = 421.6$ ppm; ^{183}W NMR (DMF/CD_3COCD_3): $\delta = -116.5$ (2W), -139.0 (2W), -146.0 (1W), -163.2 (2W), -174.4 (2W), -182.3 (2W), -202.9 (2W), -216.0 (2W), -300.9 ppm (2W); IR (KBr): $\tilde{\nu} = 2961$ (m), 2935 (m), 2872 (m), 1484 (m), 1381 (w), 1089 (s), 955 (s), 911 (s), 786 (s), 525 (w), 383 (m), 327 cm^{-1} (m); UV/Vis (CH_3CN): $\lambda_{max} = 455$ nm; elemental analysis calcd (%) for $C_{112}H_{252}N_8O_{61}P_2W_{17}Os$: C 22.18, H 4.19, N 1.85; found: C 21.73, H 4.20, N 1.97.

Preparation of $[(Bu_4N)_7][\alpha_1\text{-}P_2W_{17}O_{61}\{Os^{VI}N\}]$: $[Bu_4N][OsCl_4N]$ (0.204 g, 0.347 mmol) in methanol (8 mL) and distilled water (30 mL) were added to $K_{10}[\alpha_1\text{-}P_2W_{17}O_{61}]$ (1.504 g, 0.333 mmol). The mixture was stirred at room temperature in the dark. After 17 h, $(Bu_4N)Br$ (0.654 g, 2.030 mmol), acetonitrile (40 mL), CH_2Cl_2 (40 mL), and additional distilled water (50 mL) were added. The organic layer was separated (additional CH_2Cl_2 may be required to completely separate the phases), dried over anhydrous K_2CO_3, the solvents were removed in vacuo, and the product was washed once with diethyl ether. Yield: 1.355 g. This black solid was found to be $[(Bu_4N)_7][\alpha_1\text{-}P_2W_{17}O_{61}\{Os^{VI}N\}]$ contaminated with approximately 19% of $[(Bu_4N)_6][\alpha\text{-}P_2W_{18}O_{62}]$ as judged by using ^{31}P NMR spectroscopy ($\delta = -11.9$ ppm). ^{31}P NMR (CD_3CN): $\delta = -11.5$,

−12.3 ppm; ^{15}N NMR (CH_3CN/CD_3CN): $\delta = 441.6$ ppm; ^{183}W NMR (CH_3CN/CD_3CN): $\delta = -102.3$ (1W), −106.8 (1W), −115.3 (1W), −132.1 (1W), −157.2 (1W), −160.0 (2W), −161.4 (1W), −168.3 (1W), −174.4 (3W), −178.6 (1W), −192.7 (1W), −206.2 (1W), −252.0 (1W), −287.2 ppm (1W).

Preparation of $[(Bu_4N)_4][\alpha\text{-}PW_{11}O_{39}\{Re^{VI}N\}]$

Method A: Et_3N (0.020 mL, 0.150 mmol) and $[ReCl_3(N_2Ph_2)(PPh_3)_2]$ (0.068 g, 0.059 mmol) were successively added to a solution of $[(Bu_4N)_4][\alpha\text{-}H_3PW_{11}O_{39}]$ (0.183 g, 0.050 mmol) in distilled CH_3CN (5 mL). Within a few minutes under reflux conditions, the initially brown suspension turned violet; this was left at reflux for 1 h and filtered. Deep-violet crystals were grown by means of slow diffusion of Et_2O into the filtrate. These crystals were found to be contaminated with approximately 5.3% of $[(Bu_4N)_4][\alpha\text{-}PW_{11}O_{39}\{Re^{V}O\}]$ as judged by using ^{31}P NMR spectroscopy ($\delta = -14.59$ ppm).

Method B: Et_3N (0.400 mL, 2.800 mmol) was added to a solution of $[(Bu_4N)_4][\alpha\text{-}H_3PW_{11}O_{39}]$ (0.365 g, 0.100 mmol) and $[Bu_4N][ReCl_4N]$ (0.058 g, 0.100 mmol) in distilled CH_3CN (10 mL). After a few minutes, the initially yellow solution turned violet. After the solution had been stirred for three days, deep-violet crystals of $[(Bu_4N)_4][\alpha\text{-}PW_{11}O_{39}\{Re^{VI}N\}]$ were grown by means of slow evaporation.

Instrumentation: IR spectra were recorded from KBr pellets on a Bio-Rad Win-IR FTS 165 FTIR spectrophotometer, and UV-visible spectra were recorded on a Shimadzu UV-2101 spectrophotometer. ^{31}P NMR spectra (121.5 MHz, external 85% H_3PO_4) were obtained at room temperature in 5 mm o.d. tubes on a Bruker AC 300 spectrometer equipped with a QNP probe head. The ^{183}W NMR spectrum was recorded in 10 mm o.d. tubes on a Bruker AC 300 or Bruker DRX 500 spectrometer operating at 12.5 or 20.8 MHz, respectively. The AC 300 spectrometer was equipped with a triple-resonance low-frequency VSP probe head with a ^{31}P decoupling coil. Chemical shifts were measured with respect to a 2 M Na_2WO_4 solution in alkaline D_2O by using saturated $H_4[SiW_{12}O_{40}]$ as a secondary external standard ($\delta = -103.8$ ppm).[70] The ^{31}P-decoupling experiments were performed with a B-SV3 unit operating at 121.5 MHz and equipped with a B-BM1 broad-band modulator. ^{15}N NMR spectra were recorded from 90% ^{15}N-enriched samples in 10 mm o.d. tubes on a Bruker AM 500 spectrometer operating at 50.6 MHz. They were referenced to neat CH_3NO_2 ($\delta = 0$ ppm) using CH_3CN as a secondary standard ($\delta = -135.83$ ppm). ^{183}W 2D COSY spectra were obtained at 20.8 MHz on a Bruker DRX 500 instrument by using a simple Jeener (90°–incremental delay–90°–acquisition–relaxation delay) pulse sequence. The spectral width was 3300 Hz and 3200 transients were acquired with a sum of acquisition time and relaxation delay of 500 ms. The number of stored experiments was 128 for a total spectrometer time of approximately 60 h. The data were zero-filled and apodized with sine bell functions before Fourier transformation. The resulting COSY map is presented as a power spectrum after symmetrization of the transformed matrix. The $[\alpha\text{-}PW_{11}O_{39}\{Os^{VI}N\}]^{4-}$ NMR sample was obtained by dissolving $[(Bu_4N)_4][\alpha\text{-}PW_{11}O_{39}\{Os^{VI}N\}]$ (980 mg), prepared as previously described,[35] in CD_3CN (2 mL), resulting in a 1.27×10^{-1} mol L^{-1} concentration. This sample was contaminated by a very small amount of $[(Bu_4N)_3][\alpha\text{-}PW_{12}O_{40}]$ as can be seen on the ^{183}W NMR spectrum. The $[\alpha\text{-}PW_{11}O_{39}\{Re^{VII}N\}]^{3-}$ NMR sample has been obtained by dissolving $[(Bu_4N)_3][\alpha\text{-}PW_{11}O_{39}\{Re^{VII}N\}]$ (105 mg), prepared as previously described,[35] in a mixture of CH_3CN (2 mL) and CD_3COCD_3 (0.3 mL), resulting in a 1.46×10^{-2} mol L^{-1} concentration. The $[\alpha_2\text{-}P_2W_{17}O_{61}\{Os^{VI}N\}]^{7-}$ NMR sample was obtained by dissolving $[(Bu_4N)_7][\alpha_2\text{-}P_2W_{17}O_{61}\{Os^{VI}N\}]$ (760 mg) in a mixture of DMF (2 mL) and CD_3COCD_3 (0.5 mL). This sample was contaminated by approximately 40 to 50% of $[(Bu_4N)_6][\alpha\text{-}P_2W_{18}O_{62}]$ as estimated by using ^{31}P NMR spectroscopy. Consequently, there is less than 400 mg of $[(Bu_4N)_7][\alpha_2\text{-}P_2W_{17}O_{61}\{Os^{VI}N\}]$ in the NMR tube, which corresponds to a 2.64×10^{-2} mol L^{-1} concentration. The $[\alpha_1\text{-}P_2W_{17}O_{61}\{Os^{VI}N\}]^{7-}$ sample was obtained by dissolving $[(Bu_4N)_7][\alpha_1\text{-}P_2W_{17}O_{61}\{Os^{VI}N\}]$ (1.10 g) in a mixture of CH_3CN (2 mL) and CD_3CN (0.5 mL). This sample was contaminated by approximately 15% of $[\alpha\text{-}P_2W_{18}O_{62}]^{6-}$ as estimated by using ^{31}P NMR spectroscopy. X-band EPR spectra were recorded on a Bruker ESR 300 X-band spectrometer. A microwave power of 4 mW was used with a modulation amplitude of 0.5 mT. The 190 GHz spectra were obtained on a standard HF-EPR Grenoble spectrometer.[71,72] Spectra of frozen and powdered samples were recorded at 90 K for X-band and at 5 K for 190 GHz. Spectra processing was performed with software provided by Bruker, whereas simulation of the spectra was carried out with the EPRsim32[73] and SIMPIPM programs.[74] For the least-squares optimization a hybrid genetic algorithm, combined with Powell refining and the Simplex method, was used. Electrochemical data were recorded in acetonitrile, with sample concentrations of 10^{-3} M and 0.1 M $(Bu_4N)BF_4$ as the supporting electrolyte. Cyclic voltammetry at a carbon electrode was carried out on a PAR model 273 instrument. A standard three-electrode cell was used, which consisted of the working electrode, an auxiliary platinum electrode and an aqueous saturated calomel electrode (SCE) equipped with a double junction. All potentials are relative to the SCE. The ESI mass spectra were recorded by using an ion-trap mass spectrometer (Bruker Esquire 3000, Bremen, Germany) equipped with an orthogonal ESI source. The capillary high voltage was set to +3500 V. The capillary exit, skimmer 1 and skimmer 2, were typically set to (−)80, (−)25, and (−)6 V, respectively, in order to avoid in-source decomposition. Sample solutions (10 pmol μL^{-1} in acetonitrile) were infused into the ESI source by using a syringe pump at a flow rate of 120 μL h^{-1}. A low declustering potential ($\Delta_{CE\text{-}Sk} = 40$ V) was used to keep the POM intact.

Acknowledgements

The authors thank Dr. Carlos Afonso for recording the ESI mass spectra of $[(Bu_4N)_4][\alpha\text{-}PW_{11}O_{39}\{Re^{VI}N\}]$, Dr. Anne-Laure Barra and Bernard Morin for recording the 190 GHz and X-band EPR spectra, respectively. University Pierre et Marie Curie and the CNRS are acknowledged for their funding, as is the U.S. DOE (DE-FG02–98ER14866). We also thank the CNRS and the NSF for supporting the nitrido-polyoxometalates with joint program 10770. Z. Sojka thanks UPMC for a one month position as invited professor.

[1] M. T. Pope, *Heteropoly and Isopoly Oxometalates*, Springer, New York, **1983**.
[2] *Polyoxometalates: From Platonic Solids to Anti Retroviral Activity* (Eds.: M. T. Pope, A. Müller), Kluwer, Dordrecht, **1994**.
[3] C. L. Hill, *Chem. Rev.* **1998**, *98*, 1–389 (topical issue on polyoxometalates).
[4] *Polyoxometalate Chemistry: From Topology via Self-Assembly to Applications* (Eds.: M. T. Pope, A. Müller), Kluwer, Dordrecht, **2001**.
[5] *Polyoxometalate Chemistry for Nano-Composite Design*, (Eds.: T. Yamase, M. T. Pope), Kluwer, Dordrecht, **2002**.
[6] C. Sanchez, G. J. de Soler-Illia, F. Ribot, T. Lalot, C. R. Mayer, V. Cabuil, *Chem. Mater.* **2001**, *13*, 3061–3083.
[7] E. Coronado, P. Day, *Chem. Rev.* **2004**, *104*, 5419–5448.
[8] S. Uchida, M. Hashimoto, N. Mizuno, *Angew. Chem.* **2002**, *114*, 2938–2941; *Angew. Chem. Int. Ed.* **2002**, *41*, 2814–2817.
[9] R. Kawamoto, S. Uchida, N. Mizuno, *J. Am. Chem. Soc.* **2005**, *127*, 10560–10567.
[10] C. R. Mayer, R. Thouvenot, T. Lalot, *Chem. Mater.* **2000**, *12*, 257–260.
[11] A. R. Moore, H. Kwen, A. M. Beatty, E. A. Maatta, *Chem. Commun.* **2000**, 1793–1794.
[12] L. Xu, M. Lu, B. Xu, Y. Wei, Z. Peng, D. R. Powell, *Angew. Chem.* **2002**, *114*, 4303–4306; *Angew. Chem. Int. Ed.* **2002**, *41*, 4129–4132.
[13] M. Lu, B. Xie, J. Kang, F.-C. Chen, Y. Yang, Z. Peng, *Chem. Mater.* **2005**, *17*, 402–408.
[14] A. Proust, R. Thouvenot, M. Chaussade, F. Robert, P. Gouzerh, *Inorg. Chim. Acta* **1994**, *224*, 81–95.
[15] A. Proust, S. Taunier, V. Artero, F. Robert, R. Thouvenot, P. Gouzerh, *Chem. Commun.* **1996**, 2195–2196.

[16] C. Bustos, B. Hasenknopf, R. Thouvenot, J. Vaissermann, A. Proust, P. Gouzerh, *Eur. J. Inorg. Chem.* **2003**, 2757–2766.
[17] J. B. Strong, R. Ostrander, A. L. Rheingold, E. A. Maatta, *J. Am. Chem. Soc.* **1994**, *116*, 3601–3602.
[18] J. L. Stark, A. L. Rheingold, E. A. Maatta, *J. Chem. Soc. Chem. Commun.* **1995**, 1165–1166.
[19] J. B. Strong, G. P. A. Yap, R. Ostrander, L. M. Liable-Sands, A. L. Rheingold, R. Thouvenot, P. Gouzerh, E. A. Maatta, *J. Am. Chem. Soc.* **2000**, *122*, 639–649.
[20] J. L. Stark, V. G. Young, Jr., E. A. Maatta, *Angew. Chem.* **1995**, *107*, 2751–2753; *Angew. Chem. Int. Ed. Engl.* **1995**, *34*, 2547–2548.
[21] C. Dablemont, A. Proust, R. Thouvenot, C. Afonso, F. Fournier, J.-C. Tabet, *Dalton Trans.* **2005**, 1831–1841.
[22] C. Dablemont, A. Proust, R. Thouvenot, C. Afonso, F. Fournier, J.-C. Tabet, *Inorg. Chem.* **2004**, *43*, 3514–3520.
[23] R. A. Eikey, M. M. Abu-Omar, *Coord. Chem. Rev.* **2003**, *243*, 83–124.
[24] D. V. Yandulov, R. R. Schrock, *Science* **2003**, *301*, 76–78.
[25] R. R. Schrock, *Chem. Commun.* **2003**, 2389–2391.
[26] J. T. Groves, T. Takahashi, *J. Am. Chem. Soc.* **1983**, *105*, 2073–2074.
[27] S. K.-Y. Leung, J.-S. Huang, J.-L. Liang, C.-M. Che, Z.-Y. Zhou, *Angew. Chem.* **2003**, *115*, 354–357; *Angew. Chem. Int. Ed.* **2003**, *42*, 340–343.
[28] G. Golubkov, Z. Gross, *J. Am. Chem. Soc.* **2005**, *127*, 3258–3259.
[29] G. Golubkov, Z. Gross, *Angew. Chem.* **2003**, *115*, 4645–4648; *Angew. Chem. Int. Ed.* **2003**, *42*, 4507–4510.
[30] T. Birk, J. Bendix, *Inorg. Chem.* **2003**, *42*, 7608–7615.
[31] J. Du Bois, C. S. Tomooka, J. Hong, E. M. Carreira, *Acc. Chem. Res.* **1997**, *30*, 364–372.
[32] W.-L. Man, W. W. Y. Lam, S.-M. Yiu, T.-C. Lau, S.-M. Peng, *J. Am. Chem. Soc.* **2004**, *126*, 15336–15337.
[33] H. Kang, J. Zubieta, *J. Chem. Soc. Chem. Commun.* **1988**, 1192–1193.
[34] M. J. Abrams, C. E. Costello, S. N. Shaikh, J. Zubieta, *Inorg. Chim. Acta* **1991**, *180*, 9–11.
[35] H. Kwen, S. Tomlinson, E. A. Maatta, C. Dablemont, R. Thouvenot, A. Proust, P. Gouzerh, *Chem. Commun.* **2002**, 2970–2971.
[36] F. Ortéga, M. T. Pope, *Inorg. Chem.* **1984**, *23*, 3292–3297.
[37] P. T. Meiklejohn, M. T. Pope, R. A. Prados, *J. Am. Chem. Soc.* **1974**, *96*, 6779–6781.
[38] J. J. Altenau, M. T. Pope, R. A. Prados, H. So, *Inorg. Chem.* **1975**, *14*, 417–421.
[39] U. Abram, M. Braun, S. Abram, R. Kirmse, A. Voigt, *J. Chem. Soc. Dalton Trans.* **1998**, 231–238.
[40] J. R. Dilworth, P. Jobanputra, J. R. Miller, S. J. Parrott, Q. Chen, J. Zubieta, *Polyhedron* **1993**, *12*, 513–522.
[41] J. Chatt, J. D. Garforth, N. P. Johnson, G. A. Rowe, *J. Chem. Soc.* **1964**, 1012–1020.
[42] B. P. Sullivan, J. C. Brewer, H. B. Gray, D. Linebarrier, J. M. Mayer, *Inorg. Synth.* **1992**, *29*, 146–150.
[43] C. Rocchiccioli-Deltcheff, R. Thouvenot, R. Franck, *Spectrochim. Acta Part A* **1976**, *32*, 587–597.
[44] C. Rocchiccioli-Deltcheff, M. Fournier, R. Franck, R. Thouvenot, *Inorg. Chem.* **1983**, *22*, 207–216.
[45] R. Thouvenot, M. Fournier, R. Franck, C. Rocchiccioli-Deltcheff, *Inorg. Chem.* **1984**, *23*, 598–605.
[46] C. Rocchiccioli-Deltcheff, R. Thouvenot, *Spectrosc. Lett.* **1979**, *12*, 127–138.
[47] R. Contant, R. Thouvenot, *Inorg. Chim. Acta* **1993**, *212*, 41–50.
[48] C. Rocchiccioli-Deltcheff, R. Thouvenot, *J. Chem. Res. Synop.* **1977**, 46–47.
[49] R. Thouvenot, M. Michelon, A. Tézé, G. Hervé in *Polyoxometalates: From Platonic Solids to Anti-Retroviral Activity* (Eds.: M. T. Pope, A. Müller), **1994**, pp. 177–190.
[50] C. R. Mayer, R. Thouvenot, *J. Chem. Soc. Dalton Trans.* **1998**, 7–14.
[51] G. Lenoble, B. Hasenknopf, R. Thouvenot, *J. Am. Chem. Soc.* **2006**, *128*, 5735–5744.
[52] R. Contant, R. Thouvenot, Y. Dromzée, A. Proust, P. Gouzerh, *J. Cluster Sci.* **2006**, *17*, 317–331.
[53] P. J. Domaille, *J. Am. Chem. Soc.* **1984**, *106*, 7677–7687.
[54] C. Rong, M. T. Pope, *J. Am. Chem. Soc.* **1992**, *114*, 2932–2938.
[55] A. Proust, M. Fournier, R. Thouvenot, P. Gouzerh, *Inorg. Chim. Acta* **1994**, *215*, 61–66.
[56] M. Abbessi, R. Contant, R. Thouvenot, G. Hervé, *Inorg. Chem.* **1991**, *30*, 1695–1702.
[57] E. Cadot, R. Thouvenot, A. Tézé, G. Hervé, *Inorg. Chem.* **1992**, *31*, 4128–4133.
[58] R. Contant, M. Abbessi, R. Thouvenot, G. Hervé, *Inorg. Chem.* **2004**, *43*, 3597–3604.
[59] N. N. Sveshnikov, M. T. Pope, *Inorg. Chem.* **2000**, *39*, 591–594.
[60] R. I. Maksimovskaya, M. A. Fedotov, G. M. Maksimov, *Izv. Akad. Nauk SSSR, Ser. Khim.* **1983**, 252–254.
[61] A. Venturelli, M. J. Nilges, A. Smirnov, R. L. Belford, L. C. Francesconi, *J. Chem. Soc. Dalton Trans.* **1999**, 301–310.
[62] G. M. Lack, J. F. Gibson, *J. Mol. Struct.* **1978**, *46*, 299–306.
[63] A. Voigt, U. Abram, R. Bottcher, U. Richter, J. Reinhold, R. Kirmse, *Chem. Phys.* **2000**, *253*, 171–181.
[64] N. G. Connelly, W. E. Geiger, G. A. Lane, S. J. Raven, P. H. Rieger, *J. Am. Chem. Soc.* **1986**, *108*, 6219–6224.
[65] F. E. Mabbs, D. Collison, *Electron Paramagnetic Resonance of d Transition Metal Compounds*, Elsevier, Amsterdam, **1992**.
[66] L. P. Kazansky, B. R. McGarvey, *Coord. Chem. Rev.* **1999**, *188*, 157–210.
[67] W. J. Randall, D. K. Lyon, P. J. Domaille, R. G. Finke, A. M. Khenkin, C. Hill, *Inorg. Synth.* **1998**, *32*, 242–268.
[68] E. Radkov, R. H. Beer, *Polyhedron* **1995**, *14*, 2139–2143.
[69] W. P. Griffith, D. Pawson, *J. Chem. Soc. Dalton Trans.* **1973**, 1315–1320.
[70] R. Acerete, C. F. Hammer, L. C. W. Baker, *J. Am. Chem. Soc.* **1979**, *101*, 267–269.
[71] F. Muller, M. A. Hopkins, N. Coron, M. Grynberg, L. C. Brunel, G. Martinez, *Rev. Sci. Instrum.* **1989**, *60*, 3681–3684.
[72] A.-L. Barra, L. C. Brunel, J. B. Robert, *Chem. Phys. Lett.* **1990**, *165*, 107–109.
[73] T. Spalek, P. Pietrzyk, Z. Sojka, *J. Chem. Inf. Comput. Sci.* **2005**, *45*, 18–29.
[74] M. J. Nilges, SIMPIPM, Illinois EPR Center, University of Illinois, **1979**.

Received: June 30, 2006

